On-orbit calibration of the Swift Ultraviolet/Optical Telescope (UVOT)

M. Ivanushkina[1], A. A. Breeveld[2], T. S. Poole[2], C. H. James[2], A. J. Blustin[2], S. R. Rosen[2], W. Landsman[3], S. D. Hunsberger[1], P. W. A. Roming[1], C. Gronwall[1], K. O. Mason[2], S. Holland[3], K. McGowan[2], M. de Pasquale[2], M. Still[3], P. Boyd[3]

[1]Pennsylvania State University, 2582 Gateway Dr. State Collage, PA 16801, USA
[2]Mullard Space Science Laboratory, UCL, Holmbury St. Mary, Dorking, Surrey, RH5 6NT, UK
[3]NASA/Goddard Space Flight Center, Code 660.1, Greenbelt, MD 20771, USA

ABSTRACT

The Ultraviolet and Optical telescope (UVOT) is one of the three instruments on board of the *SWIFT* observatory. UVOT is on the cutting edge of our ability to observe and eventually help scientists to understand gamma-ray bursts. As any space-based telescope it requires both pre-flight and on-orbit calibrations. This paper is the first of a pair of papers presenting the initial on-board calibration of the UVOT. In particular, we'll discuss distortion, large and small scale sensitivity variations and the telescope point spread function.

INTRODUCTION

The Ultraviolet and Optical telescope (UVOT) is one of the three instruments on board of the *SWIFT* observatory. UVOT is on the cutting edge of our ability to observe and eventually help scientists to understand gamma-ray bursts. The UVOT is a 0.3m Ritchey-Chrétien telescope and provides coverage of the central 17x17 arcmin field of view in the optical or UV band (range 170-600nm), at the same time as the XRT and BAT observations. Its focal-plane detector is a micro-channel plate (MCP) intensified CCD detector. UVOT can operate in photon-timing (event) mode and/or imaging mode; it can provide half arcsecond resolution imaging of the whole field of view, and can also provide millisecond timing information. Seven broad-band filters (U, B, V, UW2, UVM2 & UW1) allow colour discrimination, and there are two grisms, one in the UV and one in the optical, to provide low resolution spectroscopy. More detailed information about *Swift* may be found in Gehrels et al. (2005)[1] and about UVOT in Roming et al. (2005)[2].
As any space-based telescope it requires both pre-flight and on-orbit calibrations. This paper is the first of a pair of papers presenting the initial on-board calibration of the UVOT. In particular, we'll discuss distortion, large and small scale sensitivity variations and the telescope point spread function.

1. DISTORTION CORRECTION

One of the main calibration tasks is a distortion correction. Alignment variation in the optical fiber taper (transmitting signal from the micro-channel plate to the CCD) creates a positional distortion. This means that detector coordinates for a group of stars does not accurately reflect their relative positions on the sky. The distortion effect is a primary source of error in determining the position for an object in the UVOT field-of-view, but it can be minimized by applying a distortion correction. A list of displacement vectors is used to "move" photon events from where they are detected to where they should be in an undistorted image. The goal of distortion analysis is to provide this list of displacement vectors to the *Swift* Science Center.
To build a set of displacement vectors, we examine detector coordinates for a set of sources whose relative positions are known. During pre-launch optical testing, we used a target mask with a pinhole grid pattern as the source input.

UV, X-Ray, and Gamma-Ray Space Instrumentation for Astronomy XIV
edited by Oswald H. W. Siegmund, Proc. of SPIE Vol. 5898
58981D, (2005) · 0277-786X/05/$15 · doi: 10.1117/12.617580

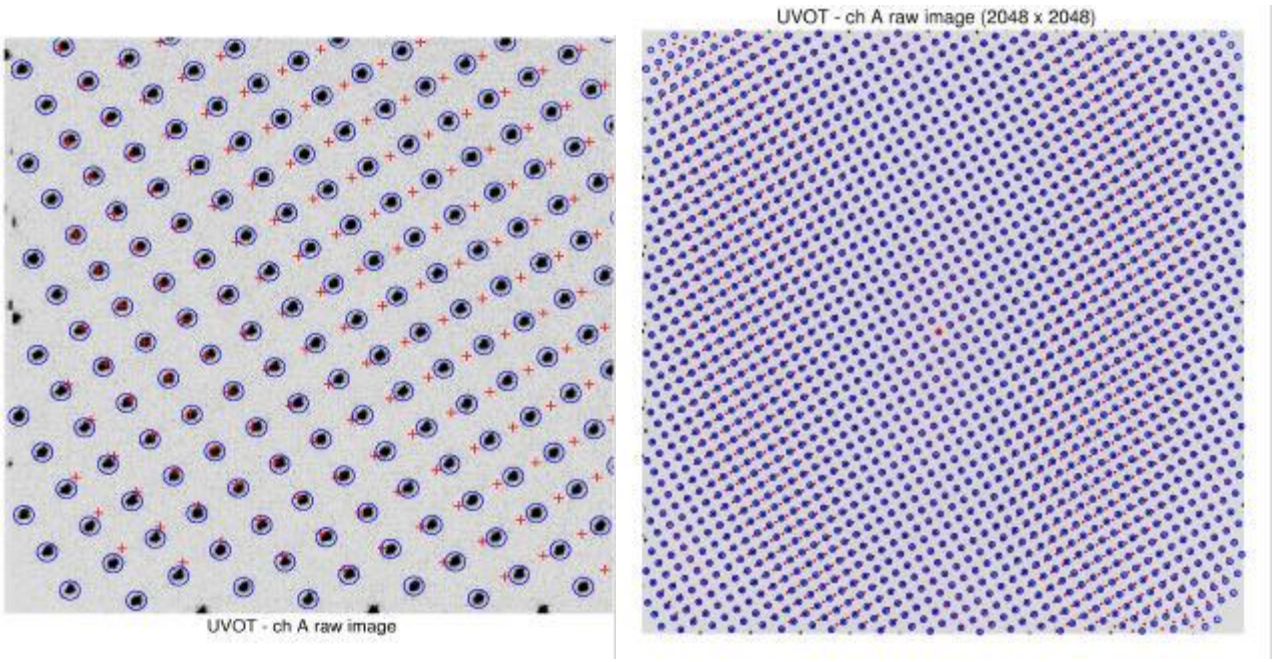

1.1 Summary of Pre-Launch Distortion Analysis

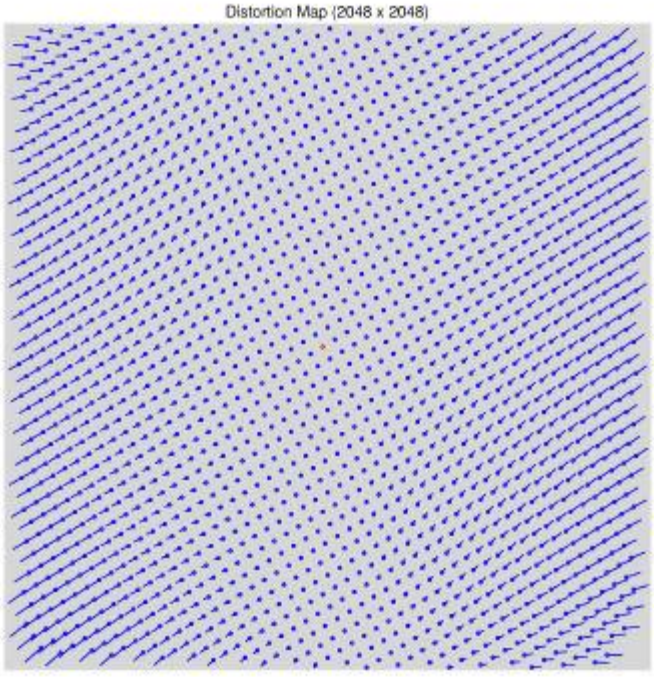

The original image (shown above) is a combination of three observations taken during optical testing. The target mask is a grid of 5µm pinholes so that an array of point sources is created. The pinholes are separated by 500µm and the grid is rotated ~30° with respect to the detector axes. The blue circles identify sources used for developing the distortion map and the red "+" signs indicate the undistorted positions of the corresponding grid points. The image on the left zooms in on a corner of the detector.

This plot presents the 1952 data points used to create a distortion correction map. The blue circles are the undistorted grid points and the lines show displacement to the corresponding image source positions. The red circle near the center is the reference point for the grid. Distortion is most extreme in the corners and edges of the detector.

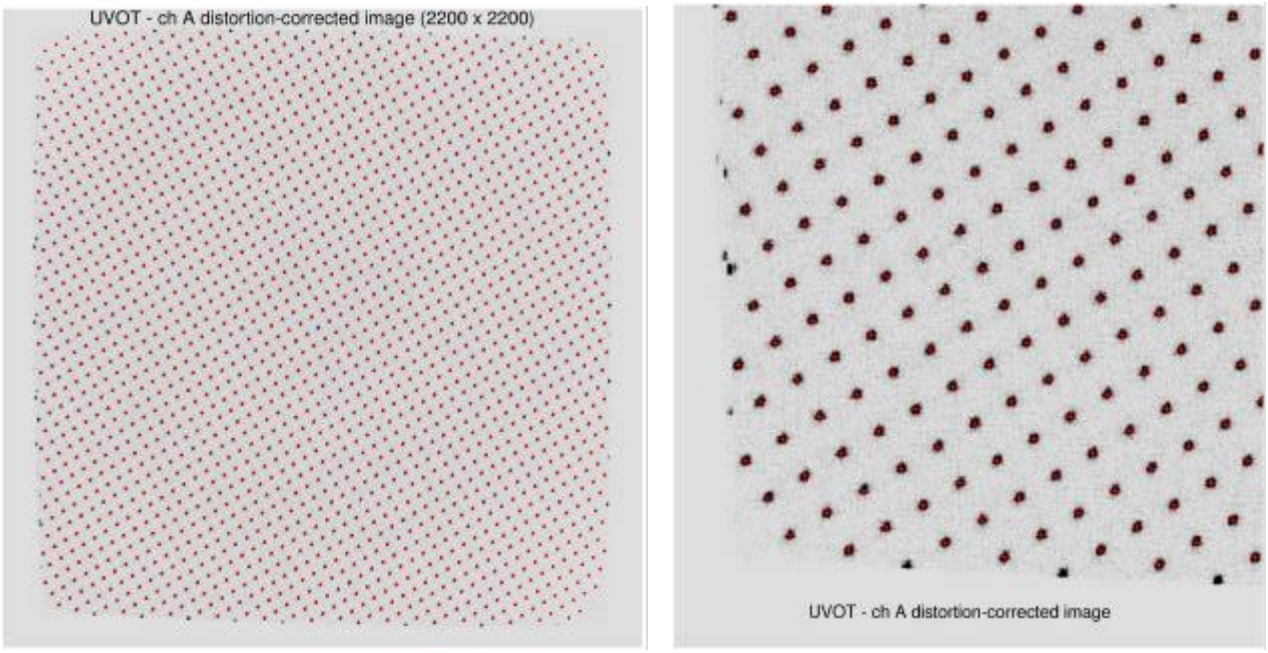

The corrected image (shown above) is produced by applying the distortion correction to the original image. Again the red "+" signs represent the undistorted positions. A close-up of the corrected image is on the right.
A simple statistical analysis yields the following information about error in the distortion correction:
the average difference between expected and corrected positions is 0.02" ± 0.03"
the median (typical) difference is 0.02"
the minimum and maximum differences are 0.00" and 1.22"
A graphical summary of the distortion distribution is highlighted in the plot below.

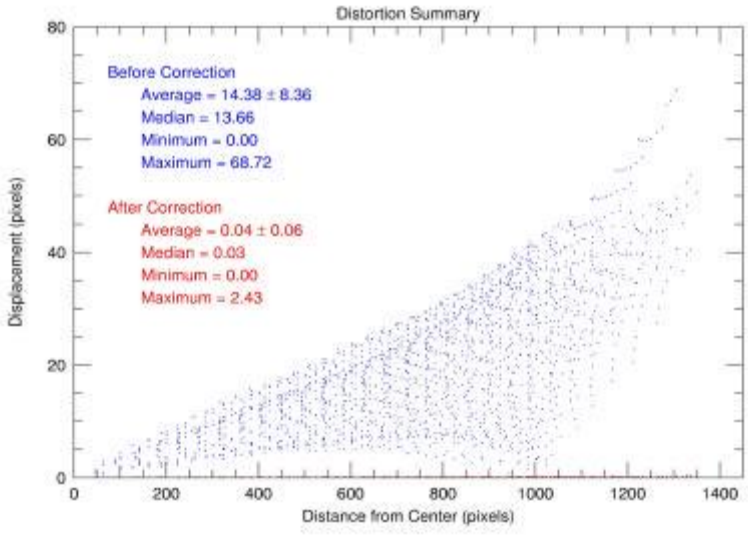

1.2 Post-launch Distortion Analysis

Initially, it is desirable to perform a distortion correction on a target star field using the map from ground-based calibration. We have created a full-frame (17' × 17') image in the V filter from photon event data processed by the *Swift* Data Center. The next step involves running a source detection program. The IRAF* tasks "daofind" and "imexamine" are suitable for use with our on-orbit data. Daofind defines the search parameters which need to be adjusted for PSF, background levels, signal-to-noise, etc. The goal is to detect as many sources as possible without getting lots of duplicates or false detections. Accurate positions are then determined with imexamine which uses the source list from daofind as input.
A variety of star catalogs are available to obtain celestial coordinates for detected sources. Digitized Sky Survey (DSS) FITS images are particularly useful because the IRAF task "xyeq" uses information in the header to convert pixel values to sky coordinates. This means we can run daofind and imexamine on the catalog images to create a source list and obtain accurate positions even for faint stars.

It is critical that the source detections on UVOT and catalog images are the same objects. Initial pattern matching is performed using a subset of bright, easily identified stars. The degree of difficulty in matching the remaining sources depends on how well the current distortion map corrects position and the number of discrepancies between the UVOT and catalog source lists. Once the matching has been completed, we can correlate the UVOT source positions to sky coordinates. Preliminary results are shown below.

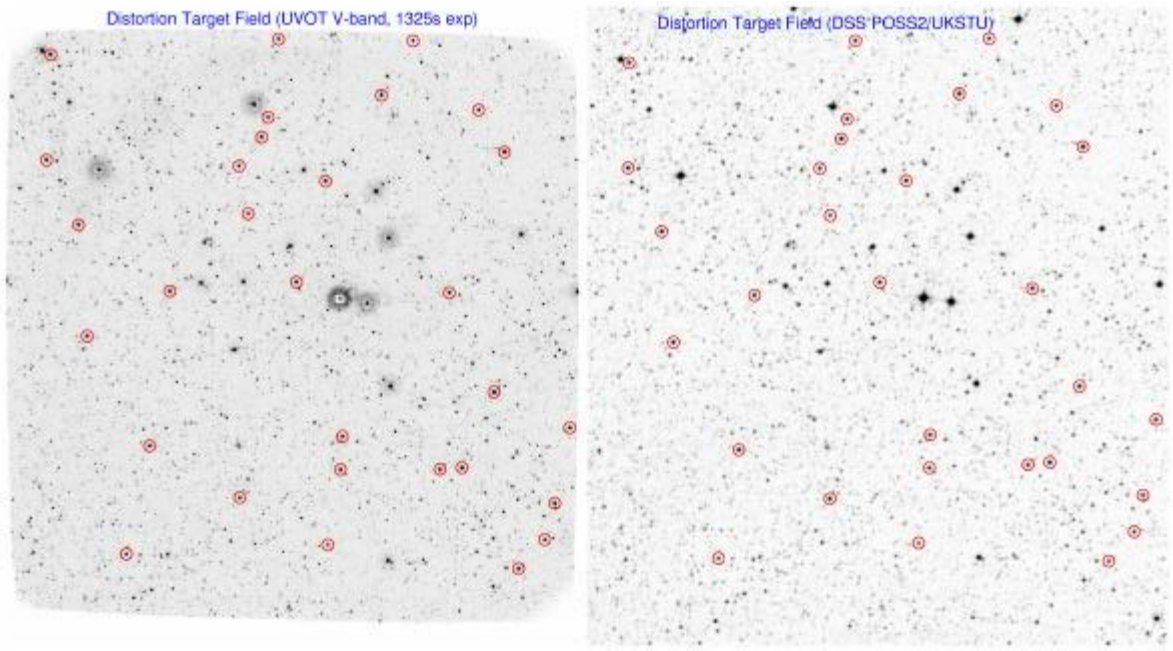

On the left is a distortion corrected UVOT image and on the right is the same field from the DSS. The red circles mark the "matched" stars. An analysis of their positional errors yields the average difference between expected and corrected positions is 0.11" ± 0.07", the median (typical) difference is 0.10", the minimum and maximum differences are 0.01" and 0.25".

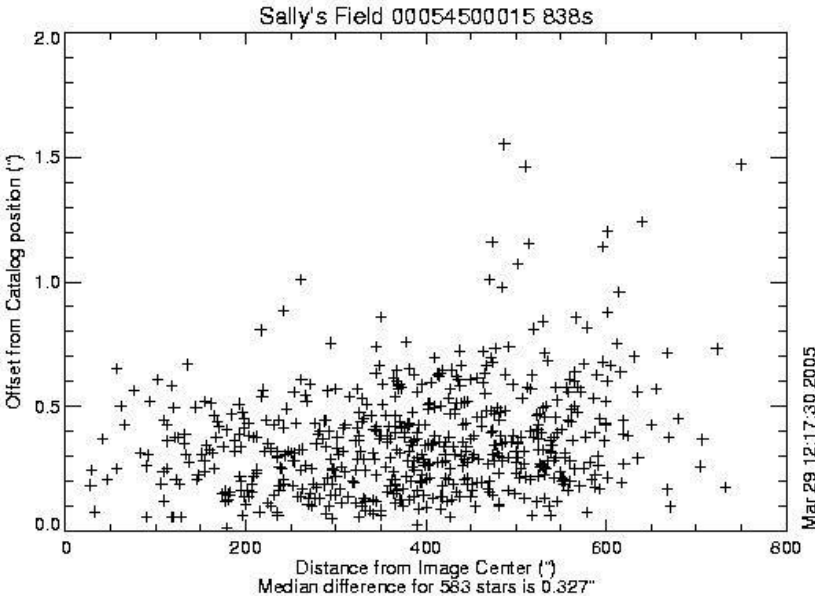

We have a teldef file based on the ground-based distortion that seems to work very well. The above plot shows that for 583 stars in the target field, the median difference between the catalog position and the position measured on the sky image is 0.327" with only a modest deterioration as one moves from the image center.

2. POINT SPREAD FUNCTION

We want to measure the point spread function (PSF) for many stars with a range of count rates to determine an optimal PSF for each filter. Target fields were chosen in which there are a significant number of isolated sources with varying count rates, but are not too over-crowded to avoid problems with measuring the PSF in the wings of the sources. We observed LH9 offset (Sally's Field) in the V, B and U filters. This field does not contain a large number of blue sources so we observed LH9-LH10 for the UVW1, UVW2 and UVM2 filters.

Filter	FWHM x (")	FWHM y (")	FWHM xy (")
V	1.76	1.82	1.79 +/- 0.05
B	1.85	1.98	1.91 +/- 0.09
U	2.02	1.90	1.96 +/- 0.08
UVW1	2.11	2.19	2.15 +/- 0.06
UVM2	1.91	1.81	1.86 +/- 0.07
UVW2	2.19	2.15	2.17 +/- 0.03

We used "Daophot" to identify and compute the centroids for the isolated stars. Photometry was performed on all of the objects found using an aperture with a radius of 6 arcsec (12 pixels) for the optical filters, and a radius of 12 arcsec (24 pixels) for the ultraviolet filters. A sub-set of the brightest sources were utilized to determine a rough analytical PSF for the frame, rejecting any sources that are too close to the edges of the frame or a brighter star. The results of the PSF fitting were employed to refine the coordinates of the detected sources. The photometry and PSF fitting were repeated using the new coordinates and a Moffat function. The PSF was computed by selecting as many of the stars as possible.

Employing the preliminary zero-points, measured in orbit, and the results from the photometry, we computed the counts in each star. The count rates were calculated using the exposure times of the observations. We have determined the final PSF for each frame by fitting all of the stars with count rates in the range 0.1 - 0.6 counts per frame. For an individual source, the main source of error on the PSF shape is the modulo 8 fixed pattern noise. This mod8 noise is due to the on-board centroiding which is used to obtain 2048x2048 subpixels from a 256x256 pixel CCD. Thus, in order to obtain a representative PSF we have had to average many point

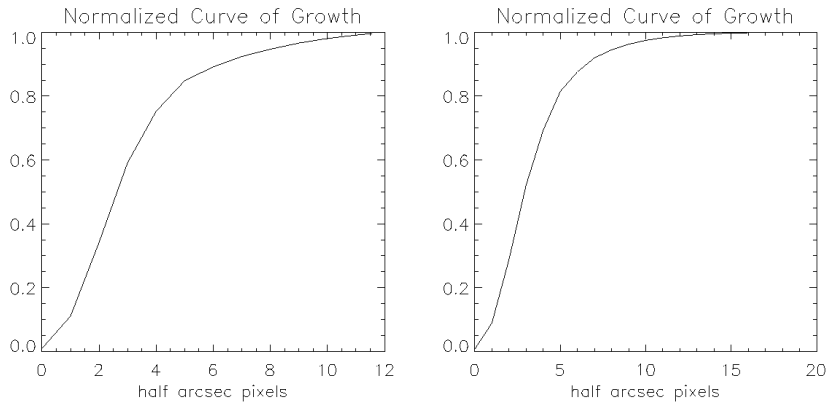

Figure 2.1 : (a) The normalized curve of growth for the V-band data.
(b) The normalized curve of growth for the UVM2-band data.

sources. We have also observed a variation (of up to 25% in the PSF FWHM) in the size of the PSF with orbit. This is probably related to temperature of the telescopes which varies with space craft voltage. Additional analysis is needed to determine how much of the source flux is gained or lost from the photometry aperture as the orbit progresses. The curve of growth was then calculated. The above method was repeated for each of the filters. We show in Figure 2.1 the normalized curve of growth for the V-band and the UVM2-band data.

3. LARGE AND SMALL SCALE VARIATIONS

3.1 Pixel-to-pixel sensitivity.

We took images with the filter in the blocked position and the LED on. The flat fields are combined to minimise the noise, obtaining 10,000 counts per CCD pixel at least. Then we binned subpixels to obtain a 256x256 image. Any large variation produced by uneven illumination of the lamp was removed by performing a large scale smoothing and then subtracting the lamp signature. Plots of counts per CCD pixel were created, and any deviations from the expected Poisson variations were noted and monitored with respect to time. As stated above, in order to have a good signal-to-noise ratio we need at least 10,000 cts/pixel. So far, the sum of exposure times in orbit has not been high enough to go beyond this value.

3.2 Large Scale Sensitivity

We have utilized the following method to determine if there are any large scale changes in sensitivity for the UVOT. We constructed a sample of V-band images that are full frame (2048 pixels x 2048 pixels), have exposure times >1000 secs, and cover as many different parts of the sky as possible. For fields that were observed more than once the images with adequate exposure times were combined using IRAF's "imcombine" to create an average of the field, scaling by the exposure time. The resulting images, and the images for the fields with single observations, were separated into three groups. The groups were determined by requiring that each one contained ~10,000 secs of data. For each group of images we employed "imcombine" to clip any data greater than 2 sigma and scale each image by its median value. The resulting images were combined to create a median of the contributing images. The three median images were then averaged, scaling by the median. The image generated by this procedure shows the large scale variations that are present in a ~1600 sec exposure V-filter observation (see Figure 3.2). The large ring feature is at a low level (approximately 7 counts per pixel in 1600 seconds). Futher work is needed to determine whether the increase in counts in the ring is due to scattered light or increased throughput in this region. At present we believe it to be due to low-level scattered light. Analysis of data from the other filters is on-going.

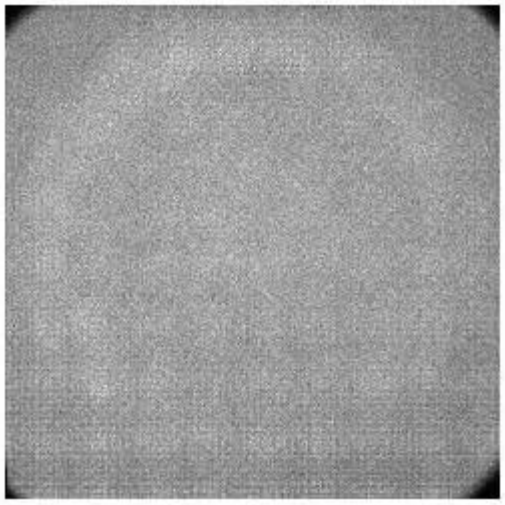

Figure 3.2 - ~1600 sec exposure V-band image resulting from the large scale sensitivity analysis.

3.3 Bad pixels

Several flat fields, for a total exposure time of about 1,000,000 sec were taken with UVOT calibration lamps. Visual inspections revealed areas of bad pixels that appear as "holes" in the background. Flat fields were combined to produce a single image. Afterwards, a numerical printout of the pixel map showed exact positions where the count rate was low or zero. These areas should correspond to those found visually. This analysis was performed both pre and post-launch.
Figure 3.3.1 is an example of the one of the flat fields obtained so far. The short exposure is insufficient to show the uneven illumination due to the LED, but we can see a reduction in the count rate at the bottom and left hand side. This is believed to be due to a shadow from the square indium ring and the sitting of the LED. The same effect is not seen in the sky flats (see 3.2) and therefore the indium ring is not blocking photons from the telescope in any way. In the images, we can see a clear dropout of the count rate towards the bottom and the left hand side of the CCD. This dropout is quite sharp.

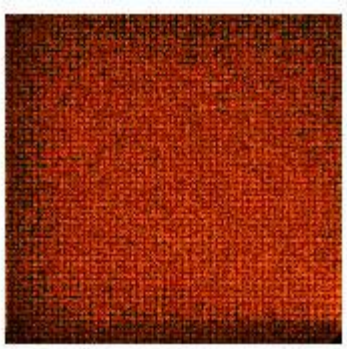

We discussed this point with MSSL engineers and we suppose that this could be due to a non-perfect alignment of the indium ring square aperture with the CCD (see Figure 3.2), which causes a shadow to be cast on fields a part of the detector. Bad pixels found in the corners of the image are due to the fact that the round fibre bundle does not completely cover the square CCD area. There are also a few subpixels in the left hand column of the image which are wrapped from the right hand column. This is due to mismatch between CCD pixel boundaries, the centroiding and the software detector window. Only this very small part of the image is affected. These will also be flagged as bad pixels. The image was electronically adjusted during testing to get the best fit. No other parts of the image are affected by this problem.

Figure 3.3.1 Flat field

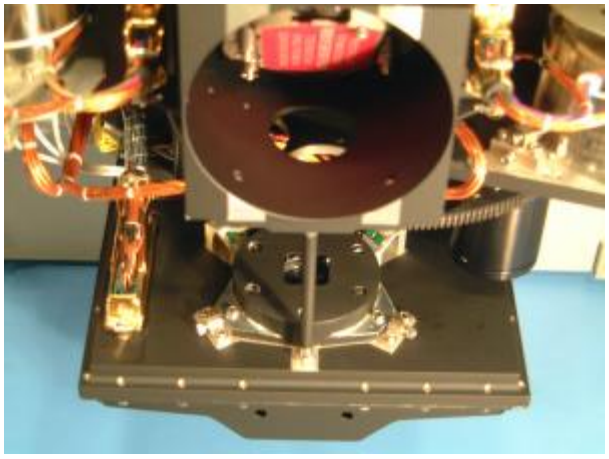

Figure 3.3.2 - The indium ring is visible at the bottom of this image. It has a square aperture.

3.4 Dark Frames

Images and event data were taken with the filter in the blocked position, after which data needed to be binned to remove some of the statistical noise. The number of events per CCD pixel per second was measured and plotted as function of time. The expected value is 4×10^{-5} counts per second per pixel. Any increase in dark count rate with time should be reported as a problem (take into account, however, that the count/rate may depend on the direction of pointing if the field contains very bright stars). The product is in the form of an image, showing dark counts as function of pixel numbers. We have also developed a tool that can take in the dark frame images and works out the count/rate, count/rate/pixel, the standard deviation in the distribution of dark pixel values, the mean statistical error in individual pixels. Several dark frame exposures have been already taken, and a mean dark count rate can be already calculated, as well as light curves may be produced. We note, however, that in order to accomplish this task properly, a bad pixel table is used in order to skip bad pixels from this count. Moreover, we need a good statistics on each separate pixel in the dark frame image, so that a total integration time of several hundreds of kiloseconds is required. As of July 2005, we have just reached the necessary observation time for this analysis.

In figure 3.3 we show an example of dark frame in 2048x2048 pixel resolution. The average count/rate/pixel is about 6×10^{-5} .

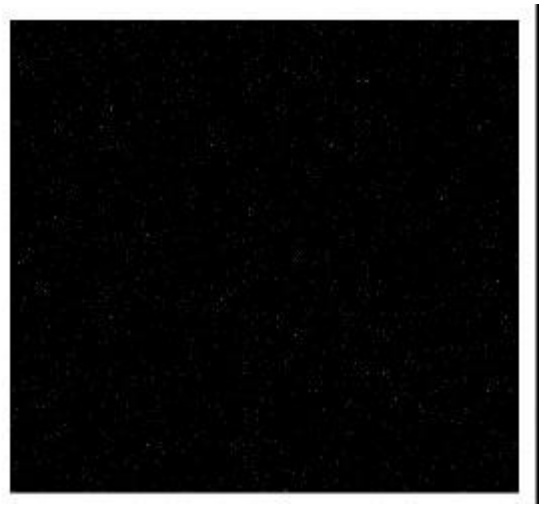

Figure 3.4 - Dark frame.

CONCLUSIONS

As any space-based telescope, *Swift* requires a thorough understanding and documentation of its capabilities and performance. On-orbit calibrations are one of the ways to ensure that data received by scientists all around the world will remain meaningful and as precise as possible. Although there has been extensive work done already toward that goal, a lot more still needs to be done. This is an on-going process that will continue throughout the mission life-time for the *Swift* telescope.

ACKNOWLEDGEMENTS

This work is supported at PSU by NASA's Office of Space Science through grant NAG5-8401 and at MSSL by funding from PPARC.

REFERENCES

1. Gehrels N. et al., ApJ 611 p1005, 2005
2. Roming P.W.A., Kennedy T.E., Mason K.O., Nousek J.A., Ahr L., Bingham R.E., Broos P.S., Carter M.J., Hancock B.K., Huckle H.E., Hunsberger S.D., Kawakami H, Killough R., Koch T.S., McLelland M.K., Smith K., Smith P.J., Soto J.C., Boyd P.T., Breeveld A.A., Holland S.T., Ivanushkina M., Pryzby M.S., Still M.D., Stock J., "The Swift Ultra-Violet/Optical Telescope", Accepted for publication in SSRev Feb 2005.
3. IRAF is distributed by the National Optical Astronomy Observatories, which are operated by the Association of Universities for Research in Astronomy, Inc. (AURA), under cooperative agreement with the National Science Foundation.
4. http://heasarc.gsfc.nasa.gov/docs/heasarc/caldb/swift/